

## Limited Stochastic Current for Energy-Optimized Switching of Spin-Transfer-Torque Magnetic Random-Access Memory

Eunchong Baek, Indra Purnama, and Chun-Yeol You<sup>✉</sup>

*Department of Emerging Materials Science, Daegu Gyeongbuk Institute of Science and Technology, Daegu, Korea*



(Received 5 August 2019; revised manuscript received 26 September 2019; published 3 December 2019)

The switching of spin-transfer-torque magnetic random-access memory (STT MRAM) in the simple macrospin model is determined by the amplitude and pulse duration of the applied current, and it requires a current that is higher than a critical current,  $I_c$ . However, this critical current misses one fundamental physical issue for the commercialization of STT MRAM; the so-called nonswitching probability ( $P_{NS}$ ) or write soft-error rate (WSER), which is influenced by the stochastic nature of the switching process at finite temperature. Herein, we propose a limited stochastic switching (LSS) current, which is another definition for the critical current with the  $P_{NS}$  incorporated. The definition of the LSS current and the analytical expressions are obtained by solving the Fokker-Planck equation with a given specific  $P_{NS}$  value. Most importantly, by using the LSS current and optimizing it together with the related pulse-duration time, we find the optimum combination of current amplitude and pulse duration, which may reduce the energy consumption of the STT MRAM by up to 75%.

DOI: 10.1103/PhysRevApplied.12.064004

### I. INTRODUCTION

In recent years, the spin-transfer-torque magnetic random-access memory (STT MRAM) has been actively studied for high-density nonvolatile memory applications [1–14]. A typical STT MRAM structure with perpendicular magnetization is shown in Fig. 1(a), where a tunneling barrier layer is sandwiched between two ferromagnetic layers that are referred to as the free layer (FL) and pinned layer (PL). The device operates by applying current to switch the magnetization states of the FL in the STT MRAM between the low-resistance state, where the magnetization of the FL and the PL are parallel to each other, and the high-resistance state where the two ferromagnetic layers have antiparallel magnetization. The switching is mediated by the spin-transfer-torque effect [3,15,16], whereby the conduction electrons of the injected current exchange their angular momentum with the local magnetization of the FL. For application purposes, the quality of STT MRAM is thus determined by the speed as well as the energy efficiency of the reading and writing processes. These factors can then be evaluated by noting the switching current, the switching time and the thermal stability of the STT MRAM. Several advances have been made to reduce the minimum current and consequently improve the energy efficiency of the STT MRAM, such as by using materials with perpendicular anisotropy [17,18], enhancing the second-order anisotropy [19], engineering

the size of the magnetic tunnel junction (MTJ) [20,21], introducing tilting PL magnetization direction [22], introducing lateral asymmetry of junction shape [23], or by introducing a strong spin-scattering layer [24,25]. Conventionally, the critical current ( $I_c$ ) that is needed to perform the FL switching can be obtained by solving the Landau-Lifshitz-Gilbert (LLG) equation with a simple macrospin model [15,26,27]. However, this method does not give us other important physical information such as the writing error rate (WER), which is the rate where the FL magnetization does not switch even when the applied current amplitude is higher than  $I_c$ . To explain this inconsistency, a new definition of critical current is needed, which takes into account the stochastic nature of the FL switching dynamics.

In this work, we propose an alternative definition of switching current, which is termed as the limited stochastic switching (LSS) current. The LSS current,  $i_{LSS}$ , is derived by solving the Fokker-Planck equation (FPE), which in turn gives us the relation between the applied LSS current and the error rate of both the writing and the reading process. We show that there is an exponential relation between the applied LSS current and the error rate of the STT MRAM, which gives us a better control over the operation error of the STT MRAM. In addition, by calculating the energy consumption using the LSS current and the corresponding pulse-duration time, we show that the most energy-efficient STT MRAM operation can be achieved when  $i_{LSS} \approx 2$  ( $I = 2I_c$ ), whereby doing so reduces the energy cost by up to 75%.

\*cyyou@dgist.ac.kr

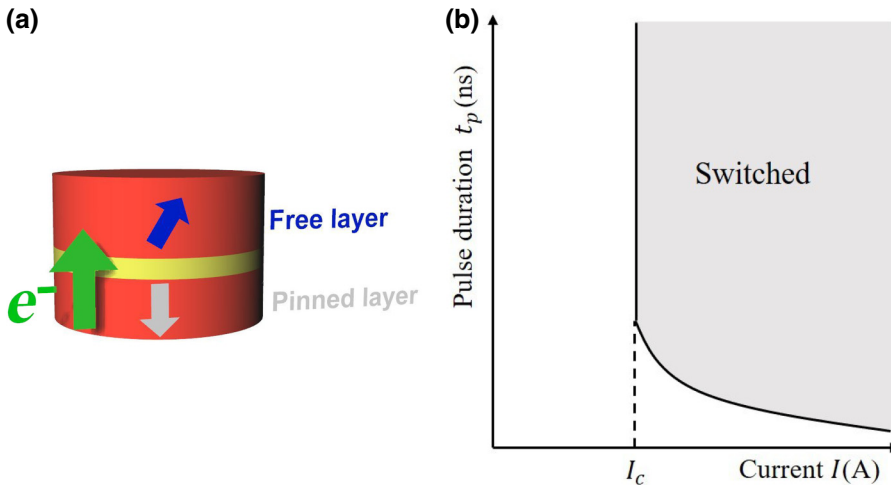


FIG. 1. (a) Schematic of the perpendicular STT MRAM. Current is applied across the device to switch the magnetization of the free layer by spin-transfer torque. (b) Conventional switching diagram with applied current and pulse duration,  $t_p$ . The magnetization is not switched in the white region.  $I_c$  is the critical current for switching in a simple macrospin model.

## II. MODEL

In this Paper, we consider a typical perpendicular STT MRAM structure as shown in Fig. 1(a). The schematic figure shows the application of current to the device in order to switch the FL magnetization from the up to the down state. We assume that the magnetization of the PL does not change when the device is under operation, which can be achieved by introducing an antiferromagnet layer underneath the PL to induce exchange bias between the PL and the antiferromagnet layer. The conventional switching diagram obtained by using the LLG equation is shown in Fig. 1(b). In this diagram, the conventional critical current  $I_c$  is shown by the solid line, which sharply separates the “switched” and the “not-switched” regions. We can then predict whether the STT MRAM switches at a given current amplitude and pulse duration by comparing the values to the critical-current line in the diagram. However, as mentioned previously, using this phase diagram as well as  $I_c$  does not give us the error rate of the device at the finite temperature.

Instead of using the LLG equation to produce the error rate, the FPE is used in this work to describe the switching dynamics statistically. Several advances have been made by using the FPE to analyze the stochastic dynamics of spin-torque-induced switching [28–33]. For instance, Matsumoto *et al.* have devised an alternative way to define the thermal stability of a nanomagnet under the influence of current [33], while Moon *et al.* have uncovered the relationship between the damping constant and the switching-time distribution of a ferromagnetic nanostructure [32]. By solving the FPE, we can obtain the magnetization switching probability under thermal fluctuation as well as under the application of current. Here it is assumed that the FL has a perpendicular uniaxial anisotropy without external magnetic field. Following the previous work by Butler *et al.* [29], the FPE for time-dependent probability distribution of magnetization as a function of the polar angle

$\theta = \cos^{-1}(m_z)$  of the FL is given by

$$\frac{\partial \rho(\theta, \tau)}{\partial \tau} = -\frac{1}{\sin \theta} \frac{\partial}{\partial \theta} \left[ \sin^2 \theta (i - \cos \theta) \rho(\theta, \tau) - \frac{1}{2\Delta} \sin \theta \frac{\partial \rho(\theta, \tau)}{\partial \theta} \right]. \quad (1)$$

Here, the field-like term of the STT and azimuthal angle dependence are not considered.  $\rho(\theta, \tau)$  is the probability of the magnetization pointing at  $\theta$  at the normalized time  $\tau = (t/t_0) = [\alpha \mu_0 \gamma H_k^{\text{eff}} / (1 + \alpha^2)]t$ , while  $i = (I/I_c) = (\eta \hbar / 2\alpha e \mu_0 H_k^{\text{eff}} M_s V) I$  is the normalized current,  $\alpha$  is the magnetic damping constant,  $H_k^{\text{eff}} = (2K_u^{\text{eff}} / \mu_0 M_s)$  is effective anisotropy field,  $\eta$  is the spin polarization of PL,  $V$  is the volume of the FL and  $M_s$  is the saturation magnetization at  $T=0$  K.  $\Delta = (K_u^{\text{eff}} V / k_B T)$  is the thermal stability factor,  $K_u^{\text{eff}} = K_u - (1/2)\mu_0 M_s^2$  is the effective uniaxial magnetic anisotropy constant while  $k_B$  is the Boltzmann constant,  $T$  is the absolute temperature, and  $K_u$  is the first-order uniaxial magnetic anisotropy constant. We consider a 40-nm-diameter Co<sub>20</sub>Fe<sub>60</sub>B<sub>20</sub>/MgO perpendicular MTJ system, where  $\alpha = 0.027$ ,  $\mu_0 H_k^{\text{eff}} = 340$  mT,  $M_s = 1.58$  T, thickness is 1 nm, and corresponding  $\Delta = 43$  for  $T = 300$  K [34]. In this dimension, the macrospin model is considered over the domain-wall model [35–38] as the macrospin model has been shown to match well with the experimental data [34]. For larger or smaller nanostructures, the accuracy of our model can be improved by using the appropriate parameterization for the shape anisotropy and the thermal stability. For those material and nanostructure parameters, we have  $1\tau = 0.62$  ns and  $1i = 88.02$   $\mu$ A.

## III. RESULTS AND DISCUSSIONS

### A. Nonswitching probability

The analytical solution of Eq. (1) can be obtained by using the ansatz solution  $\rho(\theta, \tau) = [2/W(\tau)] \exp$

$\{-[\theta^2/W(\tau)]\}$  in the limit where  $\theta$  is small. Then the nonswitching probability ( $P_{NS}$ ), i.e., the error rate of the writing process, is given by [29]

$$P_{NS}(i, \tau) = 1 - \exp \left\{ \left( \frac{\pi}{2} \right)^2 \frac{(i-1)\Delta}{1 - i \exp[2(i-1)\tau]} \right\}. \quad (2)$$

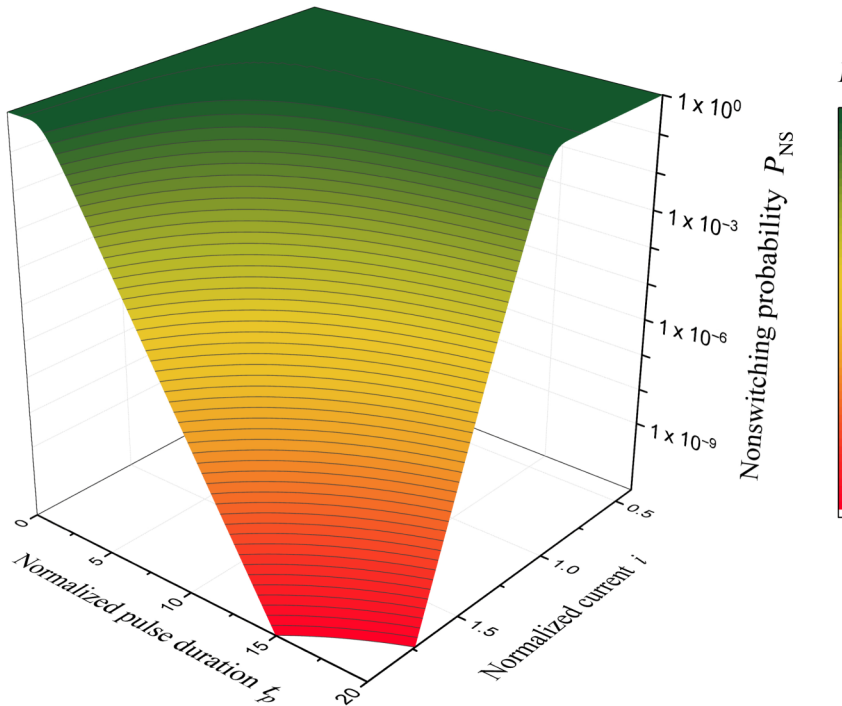
This  $P_{NS}$  is obtained by integrating  $\rho(\theta, \tau)$  from  $\theta = 0$  to  $\theta = (\pi/2)$ . We assume that the magnetization switching occurred when  $\theta > (\pi/2)$ . Figure 2 shows the error rate of the switching,  $P_{NS}$ , of the STT MRAM with  $\Delta = 60$  as a function of  $i$  and  $\tau_p$ , pulse-duration time in the unit of the normalized time  $\tau$ . Compared to the conventional switching diagram shown in Fig. 1(b), here we can see that the device has a finite nonzero  $P_{NS}$ , even with a current that is higher than the conventional critical current  $I_c$  ( $i > 1$ ).

In addition, it is also possible to calculate the error rate of the reading process. In the reading process, magnetization switching is not desired. Therefore, the error rate of the reading process is the switching probability ( $P_S$ ). By using the aforementioned method, the  $P_S$  is expressed by

$$\begin{aligned} P_S(i, \tau_p) &= 1 - P_{NS} \\ &= \exp \left\{ \left( \frac{\pi}{2} \right)^2 \frac{(i-1)\Delta}{1 - i \exp[2(i-1)\tau_p]} \right\}. \end{aligned} \quad (3)$$

Since, for reading events,  $(i-1)$  is negative, we can simplify the equation by considering  $i \times \exp[2(i-1)\tau_p] \ll 1$ .

$$P_S(i, \tau_p) = \exp \left[ \left( \frac{\pi}{2} \right)^2 (i-1)\Delta \right]. \quad (4)$$



In this case, surprisingly the  $P_S$  is independent of  $\tau_p$  and only proportional to the exponential of  $i$  and  $\Delta$ . It implies that  $P_S$  always has a finite nonzero value, and we can find the proper reading current to satisfy a specific  $P_S$  value. We discuss more details later.

### B. The limited stochastic switching current

With the above discussion in mind, it is clear that knowing the conventional critical current  $I_c$  alone is not enough for optimizing the STT MRAM working condition. Previously, as shown in Fig. 1(b), the critical-current line  $I_c$  in the conventional switching diagram is supposed to separate the region where a switching occurs or otherwise with 100% certainty. However, as shown in Fig. 2, the switching probability is not 100% even when  $i > 1$  ( $I > I_c$ ). Hence, we introduce a new definition of the LSS current for writing and reading, which considers the  $P_{NS}$  or  $P_S$  obtained by Eqs. (2) and (4), respectively.

Let us consider the LSS current for the writing event first. In this case, since the nonswitching events are undesirable only during the writing event, we assume  $i > 1$ . Then, in the limit of  $i \times \exp[(i-1)\tau_p] \gg 1$ , Eq. (2) becomes

$$P_{NS}(i, \tau_p) \approx 1 - \exp \left\{ - \left( \frac{\pi}{2} \right)^2 \frac{(i-1)\Delta}{i} \exp[-2(i-1)\tau_p] \right\}. \quad (5)$$

By performing Taylor series expansion at  $i = 2$  and noting that  $\exp[-2(i-1)\tau_p] \ll 1$ , we obtain

$$P_{NS}(i, \tau_p) \approx \left( \frac{\pi}{2} \right)^2 \frac{(i-1)\Delta}{i} \exp[-2(i-1)\tau_p], \quad (6)$$

FIG. 2. Three-dimensional surface plot with color map showing the nonswitching probability,  $P_{NS}$  as a function of the normalized applied current,  $i$ , and pulse duration,  $\tau_p$ . The thermal stability factor here is 60 and switching is assumed at  $\theta = (\pi/2)$ .

$$\ln \left[ \frac{P_{\text{NS}}}{\Delta} \left( \frac{2}{\pi} \right)^2 \right] = \ln \left( 1 - \frac{1}{i} \right) - 2(i-1)\tau_p, \quad (7)$$

$$i_{\text{LSS}}^w(P_{\text{NS}}, \tau_p) \approx 1 + \frac{2 \ln [(2\sqrt{e}/\Delta)(2/\pi)^2 P_{\text{NS}}]}{-4\tau_p + 1}. \quad (8)$$

By using the above definition,  $i_{\text{LSS}}^w$  gives us the information of how much current is needed for the device to operate with a specific nonswitching probability value at a given pulse duration. The LSS current is proportional to the natural logarithm of  $P_{\text{NS}}$  and inversely proportional to  $\tau_p$ . Figure 3(a) shows  $i_{\text{LSS}}^w$  as a function of  $\tau_p$  in a logarithmic scale for various values of  $P_{\text{NS}}$  with  $\Delta = 60$ . The result shows that depending on the  $P_{\text{NS}}$ ,  $i_{\text{LSS}}^w$  can be more than

double. The dotted line shows the conventional critical-current line obtained by solving the LLG equation. For solving the LLG equation, we assume the same MTJ model for the FPE, then the critical time for switching is given by  $\tau_c = ((-(1/2)(i+1)\ln(1-z_0) + (1/2)(i-1)\ln(1+z_0) + \ln[1-(z_0/i)])/i^2 - 1)$ , where  $z_0$  is the initial value of  $\cos \theta$  [29,39]. If we take the inverse function of this and let the critical time be a variable, we obtain the critical-current line for a given critical time, which is a given pulse duration. The dotted line is the numerical results of those inverse functions. Since it does not consider the nonswitching events, it has a smaller value for the same  $\tau_p$  when compared to the LSS current. For both methods,  $i_{\text{LSS}}^w$  is saturated to 1 at a large enough  $\tau_p$ , as shown in Fig. 3(a). Figure 3(b) shows  $i_{\text{LSS}}^w$  increases linearly with exponential

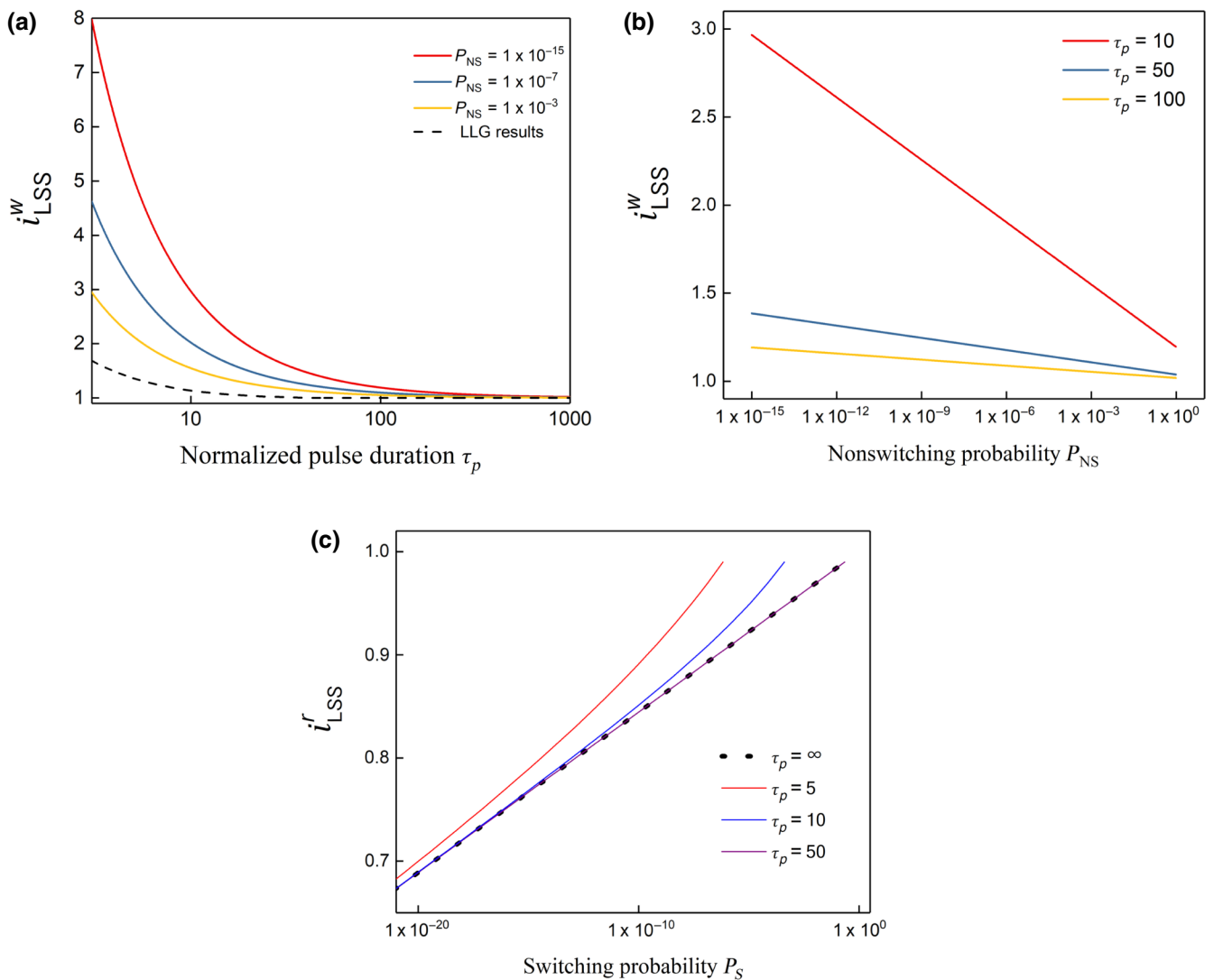


FIG. 3. (a) Limited stochastic switching current for the writing process,  $i_{\text{LSS}}^w$ , as a function of logarithmic  $\tau_p$  for various  $P_{\text{NS}}$ . The dotted line shows the result of the LLG equation, which does not consider the stochastic effect. (b)  $i_{\text{LSS}}^w$  as a function of logarithmic  $P_{\text{NS}}$  for various  $\tau_p$ . (c) Limited stochastic switching current for the reading process,  $i_{\text{LSS}}^r$ , as a function of logarithmic  $P_S$  for  $\tau_p = 5, 10$ , and  $50$ . The thermal stability factor here is 60.

decrease of  $P_{\text{NS}}$ . Depending on  $\tau_p$ , the linear increase of  $i_{\text{LSS}}^w$  has a different slope.

For the reading event, the LSS current, which takes into account the error rate  $P_S$ , can be obtained from Eq. (4) as

$$i_{\text{LSS}}^r(P_S) \approx 1 + \frac{1}{\Delta} \left( \frac{2}{\pi} \right)^2 \ln P_S. \quad (9)$$

The LSS current for the reading process is also found to be independent of  $\tau_p$  as we already mention, it is inversely proportional to  $\Delta$  and is proportional to the natural logarithm of  $P_S$ . Figure 3(c) shows  $i_{\text{LSS}}^r$  with  $\Delta = 60$ . The dotted line is the result of Eq. (9) with  $\tau_p = \infty$ , while the red, blue, and purple solid lines are numerical solutions of Eq. (3) for  $\tau_p = 5, 10$ , and  $50$ , respectively. The red and blue line has a finite difference from the dotted line at a large value of  $\ln P_S$ . However, when  $\ln P_S$  becomes smaller, there is no difference for the  $\tau_p = 10$  (blue) line, the  $\tau_p = 50$  (purple) line, and the  $\tau_p = \infty$  (dotted) line, which shows that at low reading current, the error rate is not affected by the pulse-duration time.

### C. Energy consumption of the STT MRAM under the LSS current

Up to this point, we discuss the analytical solution of the LSS current at both the writing and the reading processes. Equation (8) shows that device operation with low  $P_{\text{NS}}$  requires large amplitude of pulse current or long pulse duration. However, this has a negative impact for energy-efficient operation where the energy consumption of the device is a product of the power and the time.

Furthermore, long pulse duration implies slower operating time of the devices. Therefore, we should optimize how the current is applied by considering not only  $P_{\text{NS}}$  but also the energy consumption of the device. If we assume that the resistance of device ( $R$ ) is constant and set by  $30 \text{ k}\Omega$  [34], the energy consumption of each current pulse ( $E$ ) can then be written as  $E = P \times t = RI^2t = E_0 i^2 \tau_p$ , where  $E_0 = RI_c^2 t_0 = 0.14 \text{ pJ}$  for the 40-nm-diameter  $\text{Co}_{20}\text{Fe}_{60}\text{B}_{20}/\text{MgO}$  perpendicular MTJ system [34]. From Eq. (2), we can obtain  $\tau_p$  as a function of  $i$  for a given  $P_{\text{NS}}$  as

$$\begin{aligned} \tau_p(P_{\text{NS}}, i) \\ = \frac{\ln\{1 + (\pi/2)^2[\Delta/\ln(1 - P_{\text{NS}})](1 - i)\} - \ln i}{2(i - 1)}. \end{aligned} \quad (10)$$

Then,  $E$  as a function of  $i, P_{\text{NS}}$  is given as

$$\begin{aligned} E(P_{\text{NS}}, i) &= E_0 i^2 \tau_p(P_{\text{NS}}, i) \\ &= E_0 i^2 \left( \frac{\ln\{1 + (\pi/2)^2[\Delta/\ln(1 - P_{\text{NS}})](1 - i)\} - \ln i}{2(i - 1)} \right). \end{aligned} \quad (11)$$

Now, the energy consumption includes stochastic effect and is related to  $i$  and  $P_{\text{NS}}$ . Since  $E_0$  and  $\Delta$  are material and device parameters, if we set a specific  $P_{\text{NS}}$  value,  $E$  is directly related only to the applied current,  $i$ . Figure 4(a) shows  $E$  as a function of  $i$  for various  $P_{\text{NS}}$  and  $\Delta$ . As shown in Fig. 4(a), for  $P_{\text{NS}} = 1 \times 10^{-8}$  and  $1 \times 10^{-10}$ ,  $E$  increases sharply at  $i \approx 1$  because the pulse-duration

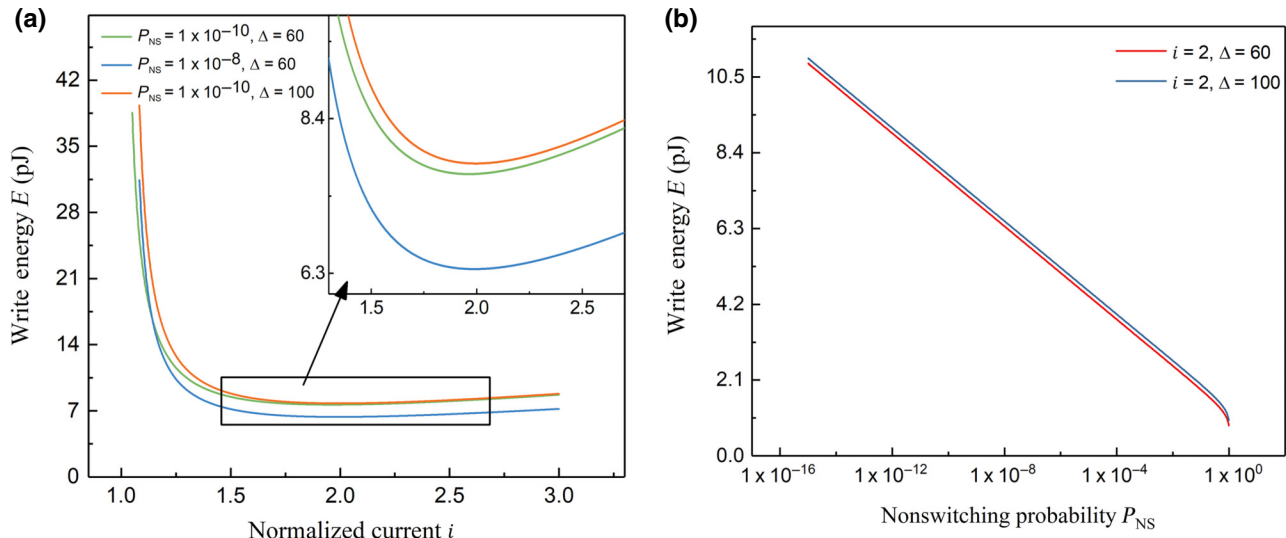


FIG. 4. (a) Energy consumption of the STT MRAM,  $E$  (pJ) as a function of  $i$  for various  $P_{\text{NS}}$  and  $\Delta$ . Inset in (a) is the enlargement of  $i = 1.3$ – $2.7$  for better comparison of a minimum point. (b)  $E$  (pJ) as a function of the nonswitching probability,  $P_{\text{NS}}$  for  $i = 2$ ,  $\Delta = 60$  and  $100$ .

time  $\tau_p$  that is needed to maintain the specific error rate increases sharply at low current, which in turn results in the sharp increase of energy usage. Most interestingly,  $E$  decreases as  $i$  increases and it has a minimum point near  $i=2$ . At this point, the energy per write cycle is approximately down to just 1/4 of the energy expenditure near  $i=1$ . This decrease in the energy expenditure,  $E$ , can be attributed to the sharp decrease of the pulse duration  $\tau_p$  that is needed to maintain the error rate  $P_{\text{NS}}$ . Beyond this point,  $E$  starts to increase again as the contribution from the  $i^2$  term starts to overcome the contribution from  $\tau_p$ . As a function of  $P_{\text{NS}}$ ,  $E$  does not have a minimum point and only increase as  $P_{\text{NS}}$  decreases [Fig. 4(b)].

The analytical solution of  $i$  where  $E$  is minimum can be obtained from Eq. (11) with the same approximation for Eqs. (5)–(8). If we set and assume that  $q \equiv (\pi/2)^2[\Delta/\ln(1 - P_{\text{NS}})] \gg 1$ , Eq. (11) becomes

$$E(P_{\text{NS}}, i) \approx E_0 \frac{i^2}{2(i-1)} \ln \left[ -q \left( 1 - \frac{1}{i} \right) \right]. \quad (12)$$

By performing Taylor series expansion at  $i = 2$ , we obtain

$$E(P_{\text{NS}}, i) \approx E_0 \frac{i^2}{4(i-1)} \left[ 2 \ln \left( -\frac{q}{2e} \right) + i \right]. \quad (13)$$

This result also supports the validity of the Taylor series expansion at  $i = 2$  throughout this Paper, because  $E$  is a minimum near  $i = 2$  regardless of  $P_{\text{NS}}$  as shown in

Fig. 4(a). From Eq. (13), we obtain  $i_{E\text{min}}$  as

$$i_{E\text{min}} = \frac{1}{4} \left\{ \sqrt{\left[ 2 \ln \left( -\frac{q}{2e} \right) + 1 \right] \left[ 2 \ln \left( -\frac{q}{2e} \right) + 9 \right]} - 2 \ln \left( -\frac{q}{2e} \right) + 3 \right\}. \quad (14)$$

Here,  $i_{E\text{min}}$  is an energy minimizing LSS current with a given  $P_{\text{NS}}$  value that is obtained by using the same approximation as Eq. (8). With the energy-minimization condition satisfied, now  $i_{E\text{min}}$  is only a function of  $P_{\text{NS}}$  instead of  $\tau_p$ . In Eq. (14), we can simplify the  $2 \ln[-(q/2e)]$  term by using the proper approximation and also by performing Puiseux series expansion [40] at  $P_{\text{NS}} = 0$  as

$$\begin{aligned} 2 \ln \left( -\frac{q}{2e} \right) &\approx 2 \left\{ \ln \left[ \left( \frac{\pi}{2} \right)^2 \frac{\Delta}{2e} \right] - \ln P_{\text{NS}} - \frac{P_{\text{NS}}}{2} \right\} \\ &\approx 2 \left\{ \ln \left[ \left( \frac{\pi}{2} \right)^2 \frac{\Delta}{2e} \right] - \ln P_{\text{NS}} \right\}. \end{aligned} \quad (15)$$

In Fig. 5(a), the solid lines show the results of Eq. (14) after replacing  $2 \ln[-(q/2e)]$  by the expression in Eq. (15) for various  $\Delta$ . As shown in Fig. 5(a),  $i$  approaches 2 at low  $P_{\text{NS}}$  regardless of  $\Delta$ .

Similar to  $i_{E\text{min}}$ , it is also possible to get the analytical solution of energy-minimizing pulse duration,  $\tau_{E\text{min}}$ . As in the case of current, the energy-minimizing pulse duration,  $\tau_{E\text{min}}$  is determined by the  $P_{\text{NS}}$ . By combining Eq. (10) with Eq. (14), we obtain  $\tau_{E\text{min}}$  as a function of  $P_{\text{NS}}$  as

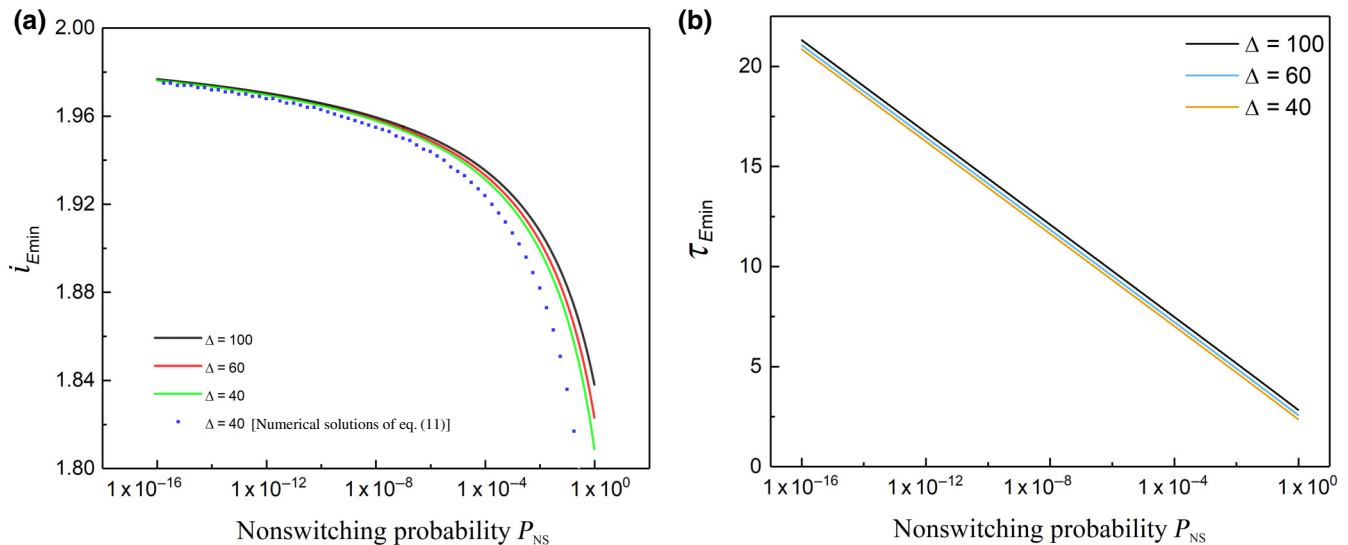


FIG. 5. (a) Limited stochastic switching current, which minimizes the energy,  $i_{E\text{min}}$  as a function of logarithmic  $P_{\text{NS}}$  for various  $\Delta$ . The solid lines show the results of Eq. (3.5) and the dotted line shows the numerical solutions of Eq. (3.2) for  $\Delta = 40$ . (b) Pulse duration at the minimum energy,  $\tau_{E\text{min}}$  as a function of logarithmic  $P_{\text{NS}}$  for various  $\Delta$ . By following these two figures, if  $P_{\text{NS}}$  is given, a set of  $(i_{E\text{min}}, \tau_{E\text{min}})$  can be determined.

$$\tau_{E \min} (P_{\text{NS}}) = \frac{1}{4} + \frac{2 \ln[-(q/2e)] + 1}{\sqrt{[2 \ln[-(q/2e)] + 1][2 \ln[-(q/2e)] + 9] - 2 \ln[-(q/2e)] - 1}} . \quad (16)$$

Figure (b) shows  $\tau_{E \min}$  increases as  $P_{\text{NS}}$  decreases while  $i_{E \min}$  approaches 2. Then, by using  $i_{E \min}$  together with the related  $\tau_{E \min}$ , we find the optimum combination of current amplitude and pulse duration for the most energy-efficient operation of the STT MRAM.

#### IV. CONCLUSION

In conclusion, we formalize an alternative perspective on the minimum current that is needed to operate STT MRAM, which is termed as LSS current. By using the LSS current formalization, we obtain a better control over the error rate during the operation of the STT MRAM. For instance, to obtain a low write soft-error rate of  $1 \times 10^{-7}$  [41], we can apply the LSS current of 0.16 mA ( $I = 2I_c$ ) with pulse duration of 6.2 ns ( $t = 10t_0$ ). Moreover, we showed that the most beneficial condition for STT MRAM operation is to apply current that is around twice that of  $I_c$ . At  $i_{\text{LSS}} \approx 2$  ( $I \approx 2I_c$ ), the energy cost per cycle is approximately 1/4 of that when  $i_{\text{LSS}} \approx 1$  ( $I \approx I_c$ ). Also, we obtain the analytical expressions of LSS current that minimizes the energy cost together with the corresponding pulse-duration conditions. Both are dependent on  $P_{\text{NS}}$  only. In this study, all relevant material parameters are represented in  $\Delta$  and  $I_c$ . Material parameterwise, the LSS current is weakly dependent on  $\Delta$  as shown in Fig. 5(a), and it should be mentioned that the LSS current is scaled by  $I_c$ . For a given  $P_{\text{NS}}$ , those analytical expressions gave us the most energy-optimized combination. This study henceforth hopes to bring a better understanding of the relation between the applied current and the error rate as well as to further improve the performance of next-generation STT MRAM.

#### ACKNOWLEDGMENTS

This work is supported by the National Research Foundation (NRF) of Korea (2015M3D1A1070465, 2017R1A2B3002621, 2017H1D3A1A01013754).

- [1] J. C. Slonczewski, Current-driven excitation of magnetic multilayers, *J. Magn. Magn. Mater.* **159**, L1 (1996).
- [2] L. Berger, Emission of spin waves by a magnetic multilayer traversed by a current, *Phys. Rev. B* **54**, 9353 (1996).
- [3] E. B. Myers, D. C. Ralph, J. A. Katine, R. N. Louie, and R. A. Buhrman, Current-induced switching of domains in magnetic multilayer devices, *Science* **285**, 867 (1999).
- [4] Y. Huai, F. Albert, P. Nguyen, M. Pakala, and T. Valet, Observation of spin-transfer switching in deep submicron-sized and low-resistance magnetic tunnel junctions, *Appl. Phys. Lett.* **84**, 3118 (2004).
- [5] H. Kubota, A. Fukushima, Y. Ootani, S. Yuasa, K. Ando, H. Maehara, K. Tsunekawa, D. D. Djayaprawira, N. Watanabe, and Y. Suzuki, Evaluation of spin-transfer switching in CoFeB-MgO-CoFeB magnetic tunnel junctions, *Jpn. J. Appl. Phys.* **44**, L1237 (2005).
- [6] K. Yakushiji, A. Fukushima, H. Kubota, M. Konoto, and S. Yuasa, Ultralow-voltage spin-transfer switching in perpendicularly magnetized magnetic tunnel junctions with synthetic antiferromagnetic reference layer, *Appl. Phys. Express* **6**, 113006 (2013).
- [7] J. C. Slonczewski, Currents, torques, and polarization factors in magnetic tunnel junctions, *Phys. Rev. B* **71**, 024411 (2005).
- [8] I. Theodosis, N. Kioussis, A. Kalitsov, M. Chshiev, and W. H. Butler, Anomalous Bias Dependence of Spin Torque in Magnetic Tunnel Junctions, *Phys. Rev. Lett.* **97**, 237205 (2006).
- [9] A. Kalitsov, M. Chshiev, I. Theodosis, N. Kioussis, and W. H. Butler, Spin-transfer torque in magnetic tunnel junctions, *Phys. Rev. B* **79**, 174416 (2009).
- [10] Z. Li, S. Zhang, Z. Diao, Y. Ding, X. Tang, D. M. Apalkov, Z. Yang, K. Kawabata, and Y. Huai, Perpendicular Spin Torques in Magnetic Tunnel Junctions, *Phys. Rev. Lett.* **100**, 246602 (2008).
- [11] D. M. Edwards, F. Federici, J. Mathon, and A. Umerski, Self-consistent theory of current-induced switching of magnetization, *Phys. Rev. B* **71**, 054407 (2005).
- [12] N. Nishimura, T. Hirai, A. Koganei, T. Ikeda, K. Okano, Y. Sekiguchi, and Y. Osada, Magnetic tunnel junction device with perpendicular magnetization films for high-density magnetic random-access memory, *J. Appl. Phys.* **91**, 5246 (2002).
- [13] S. Zhang and Z. Li, Roles of Nonequilibrium Conduction Electrons on the Magnetization Dynamics of Ferromagnets, *Phys. Rev. Lett.* **93**, 127204 (2004).
- [14] M. D. Stiles and A. Zangwill, Anatomy of spin-transfer torque, *Phys. Rev. B* **66**, 014407 (2002).
- [15] J. Z. Sun, Current-driven magnetic switching in manganite trilayer junctions, *J. Magn. Magn. Mater.* **202**, 157 (1999).
- [16] J. A. Katine, F. J. Albert, R. A. Buhrman, E. B. Myers, and D. C. Ralph, Current-Driven Magnetization Reversals and Spin-Wave Excitations in Co/Cu/Co Pillars, *Phys. Rev. Lett.* **84**, 3149 (2000).
- [17] S. Mangin, D. Ravelosona, J. A. Katine, M. J. Carey, B. D. Terris, and E. Fullerton, Current-induced magnetization reversal in nanopillars with perpendicular anisotropy, *Nat. Mater.* **5**, 210 (2006).
- [18] M. T. Rahman, A. Lyle, P. Khalili Amiri, J. Harms, B. Glass, H. Zhao, G. Rowlands, J. A. Katine, J. Langer, I. N. Krivorotov, K. L. Wang, and J. P. Wang, Reduction of switching current density in perpendicular magnetic tunnel junctions by tuning the anisotropy of the CoFeB free layer, *J. Appl. Phys.* **111**, 07C907 (2012).
- [19] R. Matsumoto, H. Arai, S. Yuasa, and H. Imamura, Efficiency of Spin-Transfer-Torque Switching and

- Thermal-Stability Factor in a Spin-Valve Nanopillar with First- and Second-Order Uniaxial Magnetic Anisotropies, *Phys. Rev. Appl.* **7**, 044005 (2017).
- [20] W. Kim, *et al.*, in *Proceedings of the IEEE International Electron Devices Meeting*, Washington, DC, 2011 (IEEE, New York, 2011), p. 24.1.1.
- [21] Y. Zhang, W. Wen, and Y. Chen, The prospect of STT-RAM scaling from readability perspective, *IEEE Trans. Magn.* **48**, 3035 (2012).
- [22] C.-Y. You, Reduced spin transfer torque switching current density with non-collinear polarizer layer magnetization in magnetic multilayer systems, *Appl. Phys. Lett.* **100**, 252413 (2012).
- [23] C.-Y. You, Reduced switching current density in spin transfer torque with lateral symmetry breaking structure, *Appl. Phys. Express* **6**, 103001 (2013).
- [24] S. Urazhdin, N. O. Birge, W. P. Pratt, Jr., and J. Bass, Switching current versus magnetoresistance in magnetic multilayer nanopillars, *Appl. Phys. Lett.* **84**, 1516 (2004).
- [25] Y. Jiang, T. Nozaki, S. Abe, T. Ochiai, A. Hirohata, N. Tezuka, and K. Inomata, Substantial reduction of critical current for magnetization switching in an exchange-biased spin valve, *Nat. Mater.* **3**, 361 (2004).
- [26] R. H. Koch, J. A. Katine, and J. Z. Sun, Time-Resolved Reversal of Spin-Transfer Switching in a Nanomagnet, *Phys. Rev. Lett.* **92**, 088302 (2004).
- [27] S. Zhang, P. M. Levy, and A. Fert, Mechanisms of Spin-Polarized Current-Driven Magnetization Switching, *Phys. Rev. Lett.* **88**, 236601 (2002).
- [28] W. F. Brown, Thermal fluctuations of a single-domain particle, *Phys. Rev.* **130**, 1677 (1963).
- [29] W. H. Butler, T. Mewes, C. K. A. Mewes, P. B. Visscher, W. H. Rippard, S. E. Russek, and R. Heindl, Switching distributions for perpendicular spin-torque devices within the macrospin approximation, *IEEE Trans. Magn.* **48**, 4684 (2012).
- [30] J. He, J. Z. Sun, and S. Zhang, Switching speed distribution of spin-torque-induced magnetic reversal, *J. Appl. Phys.* **101**, 09A501 (2007).
- [31] K.-S. Lee, S.-W. Lee, B. C. Min, and K.-J. Lee, Thermally activated switching of perpendicular magnet by spin-orbit spin torque, *Appl. Phys. Lett.* **104**, 072413 (2014).
- [32] J. H. Moon, T. Y. Lee, and C.-Y. You, Relation between switching time distribution and damping constant in magnetic nanostructure, *Sci. Rep.* **8**, 13288 (2018).
- [33] R. Matsumoto, H. Arai, S. Yuasa, and H. Imamura, Theoretical analysis of thermally activated spin transfer-torque switching in a conically magnetized nanomagnet, *Phys. Rev. B* **92**, 140409(R) (2015).
- [34] S. Ikeda, K. Miura, H. Yamamoto, K. Mizunuma, H. D. Gan, M. Endo, S. Kanai, J. Hayakawa, F. Matsukura, and H. Ohno, A perpendicular-anisotropy CoFeB-MgO magnetic tunnel junction, *Nat. Mater.* **9**, 721 (2010).
- [35] K. Munira and P. B. Visscher, Calculation of energy-barrier lowering by incoherent switching in spin-transfer torque magnetoresistive random-access memory, *J. Appl. Phys.* **117**, 17B710 (2015).
- [36] A. Meo, P. Chureemart, S. Wang, R. Chepulskyy, D. Apalkov, R. W. Chantrell, and R. F. L. Evans, Thermally nucleated magnetic reversal in CoFeB/MgO nanodots, *Sci. Rep.* **7**, 16729 (2017).
- [37] G. D. Chaves-O'Flynn, G. Wolf, J. Z. Sun, and A. D. Kent, Thermal Stability of Magnetic States in Circular Thin-Film Nanomagnets with Large Perpendicular Magnetic Anisotropy, *Phys. Rev. Appl.* **4**, 024010 (2015).
- [38] G. D. Chaves-O'Flynn, E. Vanden-Eijnden, D. L. Stein, and A. D. Kent, Energy barriers to magnetization reversal in perpendicularly magnetized thin film nanomagnets, *J. Appl. Phys.* **113**, 023912 (2013).
- [39] J. Z. Sun, Spin-current interaction with a monodomain magnetic body: A model study, *Phys. Rev. B* **62**, 570 (2000).
- [40] V. Puiseux, Recherches sur les fonctions algébriques, *J. Math. Pures Appl.* **15**, 365 (1850).
- [41] W. S. Zhao, T. Devolder, Y. Lakys, J. O. Klein, C. Chappert, and P. Mazoyer, Design considerations and strategies for high-reliable STT-MRAM, *Microelectron. Reliab.* **51**, 1454 (2011).